



## Degradation of methylene blue dye under visible light using silver/calcium hydroxide nanospheres

E.S. Aazam

Chemistry Department, Faculty of Science, King Abdulaziz University, P.O. Box 80203, Jeddah 21589, Saudi Arabia,  
email: elhamaazam@gmail.com

Received 12 September 2017; Accepted 11 January 2018

---

### ABSTRACT

A precipitation method was used to prepare nanospheres of calcium hydroxide, whereas a photoassisted deposition method was used to dope silver onto the surface of calcium hydroxide nanospheres. Silver-doped calcium hydroxide and calcium hydroxide nanospheres were characterized by several techniques. Photocatalytic degradation of methylene blue (MB) dye using visible light irradiation was used to measure the photocatalytic performance of calcium hydroxide and silver-doped calcium hydroxide nanospheres. Calcium hydroxide nanospheres absorb in the UV region; however, doping of silver onto the surface of calcium hydroxide nanospheres shifts their absorption to a longer wavelength (redshift). Additionally, by controlling the weight percentage of doped silver, the band gap of calcium hydroxide nanospheres can also be controlled. By doping 0.6 wt% of Ag, 100% of MB dye can be degraded within 30 min. In addition, 0.6 wt% Ag-doped calcium hydroxide nanospheres exhibit photocatalytic stability, showing no loss of activity after being reused five times.

*Keywords:* Calcium hydroxide; Nanospheres; Silver doping; Visible photocatalyst; MB dye

---

### 1. Introduction

The textile industry is responsible for discharging high levels of organic dyes in the environment. An estimated 15% of globally produced dyes are released through dyeing processes in textile effluents [1]. These dye effluents show characteristic fluctuating pH values accompanied by high values of chemical oxygen demand and suspended particulates. These dye substances are also known to be stable toward biodegradation and most oxidizing agents. These dye substances have detrimental effects on the aquatic ecosystem, causing eutrophication and posing risks to aquatic organisms and human health; therefore, they must be removed from the industrial effluents before discharge [2]. As international environmental regulations are becoming stricter, developing efficient technological systems for removing such dye pollutants from the wastewater stream becomes very important. The traditional techniques applied for removal of organic dyes include coagulation, chemical oxidation, adsorption, and microbial decontamination [3–5]. These treatment technologies are

very costly and require additional arrangements for removing by-products. In recent years, photocatalytic degradation has attracted substantial attention as an advanced oxidation process for efficient eradication of organic dyes and other toxic pollutants from wastewater [6].  $\text{TiO}_2$  is a widely used photocatalyst because it possesses properties that include chemical stability, nontoxicity, possible reuse, possible incorporation in other materials, and favorable physical properties. However, its wide band gap ( $E_g = 3.2$  eV) makes it active only when used in reactions that involve UV light, which constitutes approximately 3%–5% of the solar spectrum. For this reason, researchers try to manipulate the structure to narrow the band gap, making the derived material active in natural or artificial sunlight [7–20]. The use of visible radiation allows for reactions to be performed in an environmentally friendly manner without requiring energy from other sources. Scientists are interested in designing catalysts with band energies that fall within the visible frequency [21–38]. Other required properties of catalysts include nontoxicity, stability, possible reuse, ease of separation, favorable magnetic and electric properties, and

other characteristics depending on the desired application. Currently, metal hydroxide photocatalysts have also shown excellent photocatalytic properties.  $\text{In}(\text{OH})_3$  and modified  $\text{In}(\text{OH})_3$  photocatalysts exhibit high photocatalytic activity [39–41]. Additionally, calcium hydroxide can be used as an additive for dentistry and lubricants [42,43]. Calcium hydroxide exhibits photocatalytic activity in the UV region as reported in a previously published paper [44]. Therefore, the aim of this paper is to enhance the photocatalytic activity of calcium hydroxide by silver doping to shift the absorption from the UV to the visible region for methylene blue (MB) dye photocatalytic degradation.

## 2. Experimental

### 2.1. Preparation of $\text{Ca}(\text{OH})_2$ nanospheres

Solution A was prepared by dissolving anhydrous calcium chloride (20 g) in deionized water (50 mL) under stirring at room temperature. Solution B was formed by dissolving cetrimonium bromide (1 g) and NaOH (16 g) in deionized water (50 mL) under stirring at room temperature. Solution A was added to solution B under strong stirring for 60 min at room temperature. The obtained materials were washed several times with ethanol and deionized water and finally dried for 8 h at 120°C.

### 2.2. Preparation of $\text{Ag}/\text{Ca}(\text{OH})_2$ nanospheres

A photoassisted deposition method was used to dope silver onto the surface of calcium hydroxide nanospheres. Different weights of silver nitrite were dissolved in deionized water to prepare different weight percentages of silver (0.2, 0.4, 0.6, and 0.8 wt% of Ag metal). Then, the calcium hydroxide nanospheres were ultrasonically dispersed in silver nitrate solutions and the obtained mixture was exposed to UV light for 24 h. The obtained materials were washed several times in ethanol and deionized water and finally dried for 8 h at 80°C.

### 2.3. Characterization

The nanostructure of the prepared samples was examined with a JEOL-JEM-1230 transmission electron microscope (TEM). A Nova 2000 series Chromatech apparatus was employed to determine the specific surface area. A Bruker axis D8 with Cu  $K\alpha$  radiation ( $\lambda = 1.540 \text{ \AA}$ ) was applied to determine the sample phase and crystallite size. A Thermo Scientific K-ALPHA spectrometer was applied to determine the state of the silver. A spectrophotometer (V-570, Jasco, Japan) was adopted to determine the band gap of the synthesized samples. A fluorescence spectrophotometer (Shimadzu RF-5301) was applied to determine the emission spectra.

### 2.4. Photocatalytic experiment

$\text{Ag}/\text{Ca}(\text{OH})_2$  nanospheres were used to measure the degradation of MB dye using visible light. An annular batch reactor with a horizontal cylinder was used for the photocatalytic reaction. A blue fluorescent lamp with 150 W power and maximum energy, corresponding to 450 nm,

and covered by a UV cut filter was used to irradiate the  $\text{Ag}/\text{Ca}(\text{OH})_2$  nanospheres photocatalyst. The  $\text{Ag}/\text{Ca}(\text{OH})_2$  nanospheres photocatalyst was dispersed in 1,000 mL of MB dye solution with a MB concentration of 100 ppm. The photocatalytic reactions were performed at room temperature. Samples from the reaction mixture were taken at certain time interval to measure the photocatalytic activity of the  $\text{Ag}/\text{Ca}(\text{OH})_2$  nanospheres. The absorbance of the samples, analyzed by the spectrophotometer, was used to determine the remaining MB concentration in the reaction mixture. The removal efficiency of MB dye was measured by adopting the following equation:

$$\% \text{ Removal efficiency} = (C_o - C)/C_o \times 100$$

where  $C_o$  is the initial concentration of MB dye and  $C$  is the remaining concentration of MB dye.

## 3. Results and discussion

### 3.1. Photocatalyst characterization

Fig. 1 shows the XRD patterns of calcium hydroxide and silver-doped calcium hydroxide nanospheres. The results reveal that calcium hydroxide and silver-doped calcium hydroxide samples consist of calcium hydroxide. Therefore, the structure of calcium hydroxide does not change after the addition of silver. Additionally, there are no characteristic peaks for silver or silver oxide in the silver-calcium hydroxide samples either because the weight percentage of the doped silver on the surface of calcium hydroxide is below the XRD detection limit or the silver is so well dispersed on the surface of the calcium hydroxide.

XPS spectra of the Ag species for the 0.6 wt% silver-doped calcium hydroxide nanospheres sample are shown in Fig. 2. The results reveal that the state of doped silver on the surface of calcium hydroxide is metallic as indicated by the presence of two peaks for Ag  $3d_{5/2}$  and Ag  $3d_{3/2}$  at 368.1 and 374.1 eV, respectively.

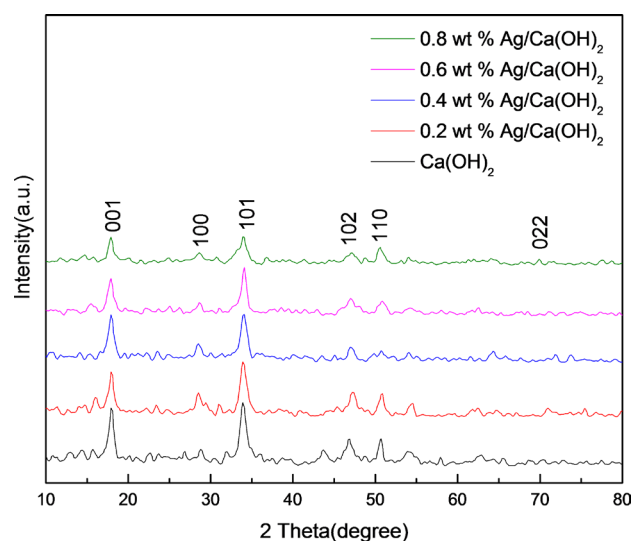


Fig. 1. XRD pattern of  $\text{Ca}(\text{OH})_2$  and  $\text{Ag}/\text{Ca}(\text{OH})_2$  nanospheres.

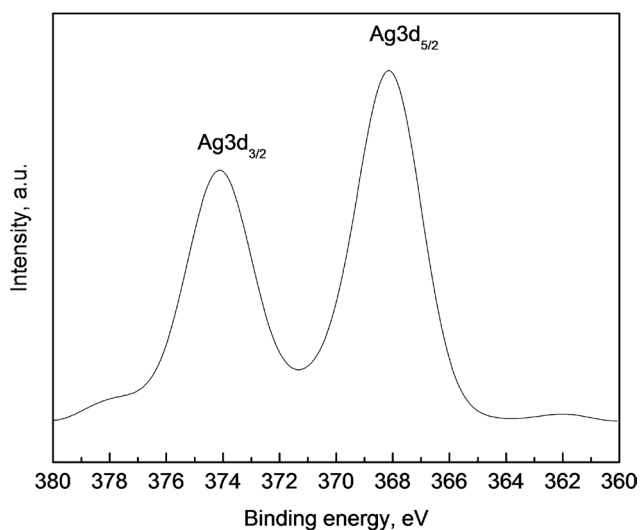


Fig. 2. XPS spectra of Ag species for 0.6 wt% Ag/Ca(OH)<sub>2</sub> nanospheres.

Fig. 3 shows TEM images of calcium hydroxide and silver-doped calcium hydroxide samples. The results reveal that the shapes of calcium hydroxide and silver-doped calcium hydroxide samples are nanospheres. Additionally, the silver doped onto the surface of the calcium hydroxide appeared as dots. The weight percentage of silver plays an important role in determining the homogeneity of doped silver, which was found to increase with increasing weight percentage of doped silver from 0.2 to 0.6 wt%. However, the homogeneity was found to decrease upon increasing the weight percentage of doped silver above 0.6 wt%.

Table S1 in the supplementary material shows the specific surface areas of calcium hydroxide and silver-doped calcium hydroxide. The results reveal that the values of the BET surface area of calcium hydroxide, 0.2 wt% Ag-calcium hydroxide, 0.4 wt% Ag-calcium hydroxide, 0.6 wt% Ag-calcium hydroxide, and 0.8 wt% Ag-calcium hydroxide are 50, 45, 42, 40, and 39 m<sup>2</sup>/g, respectively. Additionally, the BET surface area of the calcium hydroxide sample was observed to be higher than that of the silver-doped calcium hydroxide samples due to a decrease in the total pore volume of calcium hydroxide by silver doping.

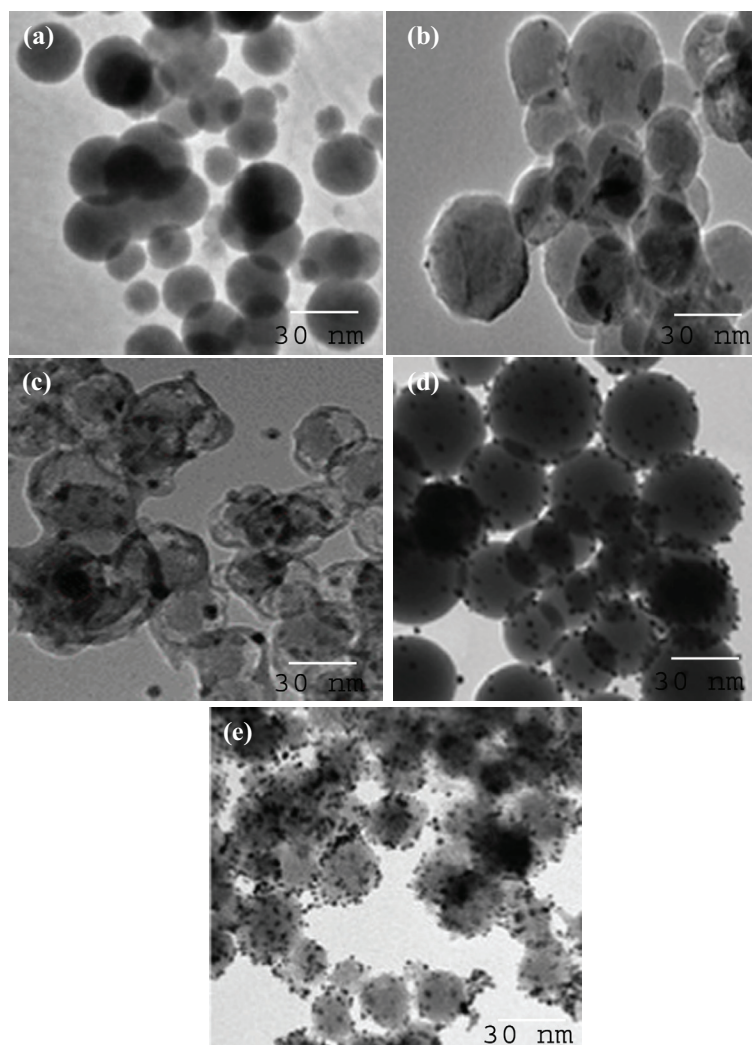


Fig. 3. TEM images of Ca(OH)<sub>2</sub> and Ag/Ca(OH)<sub>2</sub> nanospheres, where the wt% of Ag is 0 (A), 0.2 (B), 0.4 (C), 0.6 (D) and 0.8 (E).

Fig. 4 shows the UV–Vis diffuse reflectance spectra of calcium hydroxide and silver-doped calcium hydroxide nanospheres. The results reveal that calcium hydroxide nanospheres absorb in the UV region and silver-doped calcium hydroxide nanosphere samples absorb in the visible region. Furthermore, the weight percentage of doped silver plays an important role in controlling the absorption edges of the calcium hydroxide nanospheres. Table S1 demonstrates the values of the band gap energies of calcium hydroxide and silver-doped calcium hydroxide nanospheres, which were calculated from the UV–Vis spectra as published by Mohamed [20]. The band gap values of calcium hydroxide, 0.2 wt% Ag-calcium hydroxide, 0.4 wt% Ag-calcium hydroxide, 0.6 wt% Ag-calcium hydroxide, and 0.8 wt% Ag-calcium hydroxide are 3.4, 3.07, 2.99, 2.88, and 2.85 eV, respectively.

Fig. 5 shows the photoluminescence (PL) spectra of calcium hydroxide and silver-doped calcium hydroxide nanospheres. The results reveal that the calcium hydroxide nanosphere sample shows a high PL peak intensity and

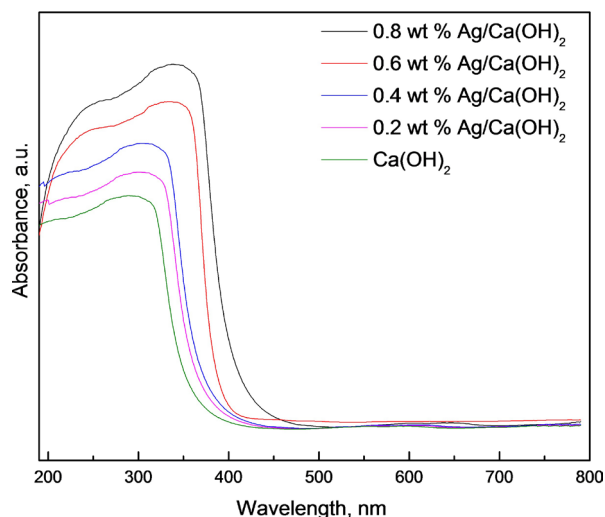


Fig. 4. UV–Vis absorption spectra of  $\text{Ca}(\text{OH})_2$  and  $\text{Ag}/\text{Ca}(\text{OH})_2$  nanospheres.

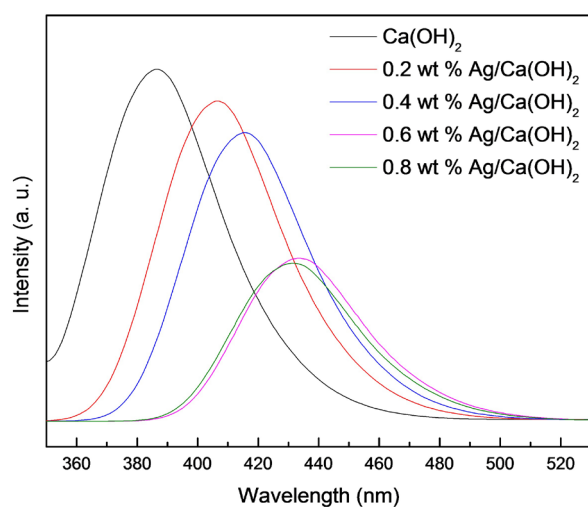


Fig. 5. PL spectra of  $\text{Ca}(\text{OH})_2$  and  $\text{Ag}/\text{Ca}(\text{OH})_2$  nanospheres.

an emission peak in the UV region, whereas silver-doped calcium hydroxide nanosphere samples exhibit a low PL peak intensity with emission peaks in the visible region. Additionally, the weight percentage of doped silver plays an important role in controlling the intensity and position of PL peaks. Therefore, the weight percentage of doped silver also plays an important role in controlling the recombination rate. The band gap values calculated from PL spectra for calcium hydroxide, 0.2 wt% Ag-calcium hydroxide, 0.4 wt% Ag-calcium hydroxide, 0.6 wt% Ag-calcium hydroxide, and 0.8 wt% Ag-calcium hydroxide are 3.3, 3.08, 2.98, 2.86, and 2.84 eV, respectively, which are in good agreement with the values calculated from the UV–Vis spectra.

### 3.2. Performance of photocatalysts for MB dye degradation

Many factors were studied to measure the photocatalytic performance of the prepared materials for MB dye degradation under visible light conditions. First, the effect of silver weight percentage on the MB dye degradation (%) was studied under the following conditions: the light source was a 500-W Xe lamp, the reaction time was 1 h, the photocatalyst dose was 0.8 g/L, the volume of aqueous solution was 1,000 mL, and the concentration of MB dye was 100 ppm. Fig. 6 shows the effect of the silver weight percentage on the MB dye degradation (%). The results reveal that the calcium hydroxide sample exhibits almost no photocatalytic activity because calcium hydroxide absorbs in the UV region and the reaction was performed under visible light. The photocatalytic performance of silver-doped calcium hydroxide nanosphere samples for MB dye degradation increased from 6% to 100% due to the decrease in the band gap of the silver-doped calcium hydroxide nanosphere samples from 3.4 to 2.88 eV by silver doping.

Second, the effect of the silver-doped calcium hydroxide photocatalyst dose on the degradation of MB dye was studied under the following conditions: the light source was a 500-W Xe lamp, the dose of the photocatalyst was changed from 0.4 to 2.0 g/L, the reaction time was 1 h, the volume of aqueous solution was 1,000 mL, and the concentration of MB dye was

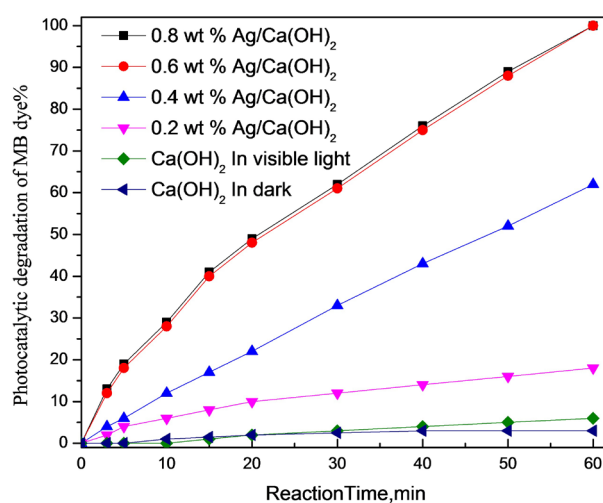


Fig. 6. Effect of wt% of Ag on photocatalytic activity of  $\text{Ca}(\text{OH})_2$  and  $\text{Ag}/\text{Ca}(\text{OH})_2$  nanospheres for methylene blue dye removal.

100 ppm. Fig. 7 shows the effect of the dose of silver-doped calcium hydroxide photocatalyst on MB dye degradation. The results reveal that the photocatalytic performance of 0.6 wt% silver-doped calcium hydroxide for MB dye degradation increased from 65% to 100% with an increase in the dose of silver-doped calcium hydroxide photocatalyst from 0.4 to 0.8 g/L. The increased dose of the photocatalyst increases the number of available sites for photocatalytic reaction, increasing the photocatalytic activity. The time required to degrade 100% of MB dye by 0.6 wt% silver-doped calcium hydroxide photocatalyst was decreased from 100 to 30 min by increasing the dose of 0.6 wt% silver-doped calcium hydroxide photocatalyst from 0.8 to 1.6 g/L. Additionally, increasing the dose of photocatalyst above 1.6 g/L was observed to decrease the photocatalytic performance of 0.6 wt% silver-doped calcium hydroxide to 98%, and the degradation time was increased again to 55 min. The high photocatalyst dose may hinder the penetration of light to the photocatalyst surface, decreasing the photocatalytic activity.

Third, the effect of the initial concentration of MB dye on the degradation of MB dye was studied under the following conditions: the light source was a 500-W Xe lamp, the reaction time was 30 min, the dose of the photocatalyst was changed to 1.6 g/L, the volume of aqueous solution was 1,000 mL, and the concentration of MB dye was changed from 25 to 200 ppm. Fig. 8 shows the effect of the initial concentration of MB dye on the MB dye degradation. The results reveal that the photocatalytic activity of 0.6 wt% silver-doped calcium hydroxide photocatalyst for all concentrations is 100%. Changing the concentration of MB dye only changed the time required to completely degrade the MB dye. The ideal initial concentration of the MB dye was 100 ppm, at which point the photocatalytic activity was 100% after 30 min.

Fourth, the recycling and reuse of 0.6 wt% silver-doped calcium hydroxide photocatalyst on MB dye degradation was studied under the following conditions: the light source was a 500-W Xe lamp, the photocatalyst dose was 1.6 g/L, the reaction time was 30 min, the volume of aqueous solution was 1,000 mL, and the MB dye concentration was 100 ppm. Fig. 9 shows the recycling and reuse of 0.6 wt% silver-doped calcium hydroxide photocatalyst on MB dye degradation. The results reveal that 0.6 wt% silver-doped calcium hydroxide photocatalyst exhibits photocatalytic stability and can be used and recycled many times.

#### 4. Conclusions

Calcium hydroxide and silver-doped calcium hydroxide nanospheres were prepared by the coprecipitation method in the presence of cetyltrimethylammonium bromide as a surfactant. The results reveal the formation of calcium hydroxide nanospheres and doped silver into a calcium hydroxide lattice. Additionally, there was a shift of the absorption edge of calcium hydroxide by the formation of a calcium hydroxide nanosphere and silver doping. The photocatalytic activity of the 0.6 wt% silver-doped calcium hydroxide nanosphere is 17-fold better than that of the calcium hydroxide nanospheres for MB dye degradation. Additionally, the 0.6 wt% silver-doped calcium hydroxide nanospheres exhibit photocatalytic stability for MB dye degradation after recycling five times.

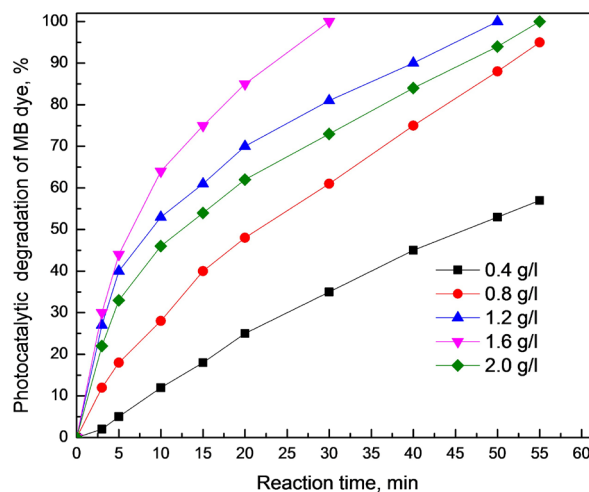


Fig. 7. Effect of loading of 0.6 wt% Ag/Ca(OH)<sub>2</sub> nanospheres on photocatalytic removal of methylene blue dye.

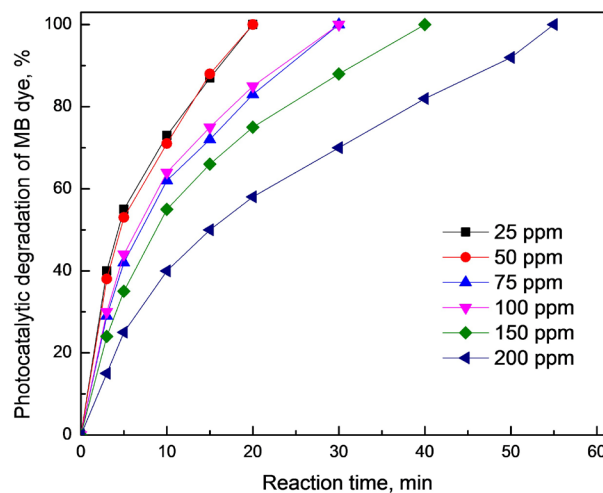


Fig. 8. Effect of initial dye concentration on the photocatalytic degradation of MB dye.

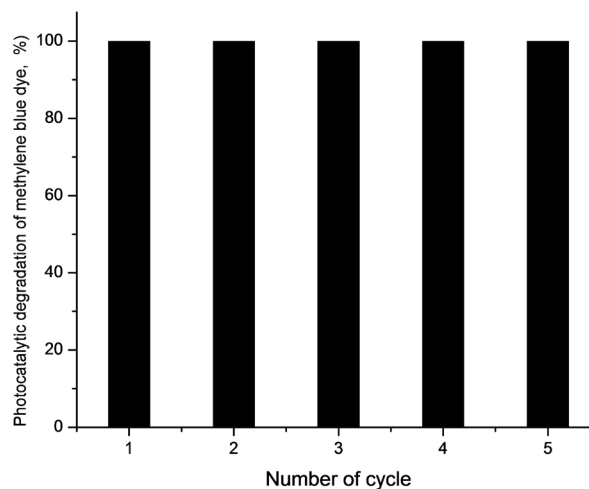


Fig. 9. Recycling and reuse of 0.6 wt% Ag/Ca(OH)<sub>2</sub> nanospheres for the photocatalytic degradation of MB dye.

## Acknowledgments

This work was funded by the Deanship of Scientific Research (DSR), King Abdulaziz University, Jeddah, under grant number (363-104-D1436). The authors, therefore, acknowledge with thanks DSR technical and financial support.

## References

- [1] C. Fernandez, M.S. Larrechi, M.P. Callao, An analytical overview of processes for removing organic dyes from wastewater effluents, *Trends Anal. Chem.*, 29 (2010) 1202–1211.
- [2] M.A. Ahmed, E.E. El-Katori, Z.H. Gharni, Photocatalytic degradation of methylene blue dye using Fe<sub>2</sub>O<sub>3</sub>/TiO<sub>2</sub> nanoparticles prepared by sol–gel method, *J. Alloys Compd.*, 553 (2013) 19–29.
- [3] K. Rajeshwar, M.E. Osugib, W. Chanmanee, C.R. Chenthamarakshan, M.V.B. Zanoni, P. Kajitvichyanukul, R. Krishnan-Ayer, Heterogeneous photocatalytic treatment of organic dyes in air and aqueous media, *J. Photochem. Photobiol., C*, 9 (2008) 171–192.
- [4] W. Nam, J. Kim, G. Han, Biodegradability of aged pyrene and phenanthrene in a natural soil, *Chemosphere*, 47 (2002) 1019–1024.
- [5] C. Guo, J. Xu, Y. He, Y. Zhang, Y. Wang, Photodegradation of rhodamine B and methyl orange over one-dimensional TiO<sub>2</sub> catalysts under simulated solar irradiation, *Appl. Surf. Sci.*, 257 (2011) 3798–3803.
- [6] A. Maleki, A.H. Mahvi, M. Alimohamadi, A. Ghasri, Advanced oxidation of phenol by ultraviolet irradiation in aqueous system, *Pak. J. Biol. Sci.*, 9 (2006) 2338–2341.
- [7] F. Atmani, A. Bensmaili, N.Y. Mezenner, Synthetic textile effluent removal by skin almonds waste, *J. Environ. Sci. Technol.*, 2 (2009) 153–69.
- [8] N. Pasukphun, S. Vinitnantharat, S. Gheewala, Investigation of decolorization of textile wastewater in an anaerobic/aerobic biological activated carbon system (A/A BAC), *Pak. J. Biol. Sci.*, 13 (2010) 316–324.
- [9] F.A. Harraz, O.E. Abdel-Salam, A.A. Mostafa, R.M. Mohamed, M. Hanafy, Rapid synthesis of titania–silica nanoparticles photocatalyst by a modified sol–gel method for cyanide degradation and heavy metals removal, *J. Alloys Compd.*, 551 (2013) 1–7.
- [10] Y. Zhang, J. Wan, Y. Ke, A novel approach of preparing TiO<sub>2</sub> films at low temperature and its application in photocatalytic degradation of methyl orange, *J. Hazard. Mater.*, 177 (2010) 750–754.
- [11] G. Tian, H. Fu, L. Jing, C. Tian, Synthesis and photocatalytic activity of stable nanocrystalline TiO<sub>2</sub> with high crystallinity and large surface area, *J. Hazard. Mater.*, 161 (2009) 1122–1130.
- [12] S. Sreekantan, L.C. Wei, Study on the formation and photocatalytic activity of titanate nanotubes synthesized via hydrothermal method, *J. Alloys Compd.*, 490 (2010) 436–442.
- [13] A.M. El-Toni, S. Yin, T. Sato, T. Ghannam, M. Al-Hoshan, M. Al-Salhi, Investigation of photocatalytic activity and UV-shielding properties for silica coated titania nanoparticles by solvothermal coating, *J. Alloys Compd.*, 508 (2010) L1–L4.
- [14] L.F. Velasco, J.B. Parra, C.O. Ania, Role of activated carbon features on the photocatalytic degradation of phenol, *Appl. Surf. Sci.*, 256 (2010) 5254–5258.
- [15] A.R. Khataee, M. Fathinia, S. Aber, M. Zarei, Optimization of photocatalytic treatment of dye solution on supported TiO<sub>2</sub> nanoparticles by central composite design: intermediates identification, *J. Hazard. Mater.*, 181 (2010) 886–897.
- [16] H.F. Yu, S.T. Yang, Enhancing thermal stability and photocatalytic activity of anatase-TiO<sub>2</sub> nanoparticles by co-doping P and Si elements, *J. Alloys Compd.*, 492 (2010) 695–700.
- [17] K. Naeem, F. Ouyang, Preparation of Fe<sup>3+</sup>-doped TiO<sub>2</sub> nanoparticles and its photocatalytic activity under UV light, *Physica B*, 405 (2010) 221–226.
- [18] E. Rossetto, D.I. Petkowicz, J.H.Z. dos Santos, S.B.C. Pergher, F.G. Penha, Bentonites impregnated with TiO<sub>2</sub> for photodegradation of methylene blue, *Appl. Clay Sci.*, 48 (2010) 602–606.
- [19] R.M. Mohamed, E.S. Baeissa, Mordenite encapsulated with Pt–TiO<sub>2</sub>: characterization and applications for photocatalytic degradation of direct blue dye, *J. Alloys Compd.*, 558 (2013) 68–72.
- [20] R.M. Mohamed, UV-assisted photocatalytic synthesis of TiO<sub>2</sub>-reduced graphene oxide with enhanced photocatalytic activity in decomposition of sarin in gas phase, *Desal. Wat. Treat.*, 50 (2012) 147–156.
- [21] W. Shu, Y. Liu, Z. Peng, K. Chen, C. Zhang, W. Chen, Synthesis and photovoltaic performance of reduced graphene oxide–TiO<sub>2</sub> nanoparticles composites by solvothermal method, *J. Alloys Compd.*, 563 (2013) 229–233.
- [22] H. Yan, S.T. Kochuveedu, L.N. Quan, S.S. Lee, D.H. Kim, Enhanced photocatalytic activity of C, F-codoped TiO<sub>2</sub> loaded with AgCl, *J. Alloys Compd.*, 560 (2013) 20–26.
- [23] Y. Cao, Z. Zhao, J. Yi, C. Ma, D. Zhou, R. Wang, C. Li, J. Qiu, Luminescence properties of Sm<sup>3+</sup>-doped TiO<sub>2</sub> nanoparticles: synthesis, characterization, and mechanism, *J. Alloys Compd.*, 554 (2013) 12–20.
- [24] R.M. Mohamed, E.S. Aazam, H<sub>2</sub> production with low CO selectivity from photocatalytic reforming of glucose on Ni/TiO<sub>2</sub>-SiO<sub>2</sub>, *Chin. J. Catal.*, 33 (2012) 247–253.
- [25] H. Zhang, C. Liang, J. Liu, Z. Tian, G. Wang, W. Cai, Defect-mediated formation of Ag cluster-doped TiO<sub>2</sub> nanoparticles for efficient photodegradation of pentachlorophenol, *Langmuir*, 28 (2012) 3938–3944.
- [26] R. Liu, P. Wang, X. Wang, H. Yu, J. Yu, UV- and visible-light photocatalytic activity of simultaneously deposited and doped Ag/Ag(I)-TiO<sub>2</sub> photocatalyst, *J. Phys. Chem. C*, 116 (2012) 17721–17728.
- [27] R.M. Mohamed, I.A. Mkhaliid, Characterization and catalytic properties of nano-sized Ag metal catalyst on TiO<sub>2</sub>-SiO<sub>2</sub> synthesized by photo-assisted deposition and impregnation methods, *J. Alloys Compd.*, 501 (2010) 301–306.
- [28] K. Chen, X. Feng, R. Hu, Y. Li, K. Xie, Y. Li, H. Gu, Effect of Ag nanoparticle size on the photoelectrochemical properties of Ag decorated TiO<sub>2</sub> nanotube arrays, *J. Alloys Compd.*, 554 (2013) 72–79.
- [29] R.M. Mohamed, I.A. Mkhaliid, The effect of rare earth dopants on the structure, surface texture and photocatalytic properties of TiO<sub>2</sub>-SiO<sub>2</sub> prepared by sol–gel method, *J. Alloys Compd.*, 501 (2010) 143–147.
- [30] R.M. Mohamed, K. Mori, H. Yamashita, Effect of Ag, Co and Cr deposit on the photocatalytic activity of titania-silica for the removal of 2-propanol in water, *Int. J. Nanopart.*, 2 (2009) 533–542.
- [31] N. Castillo, R. Pérez, M.J. Martínez-Ortiz, L. Díaz-Barriga, L. Garcia, A. Conde-Gallardo, Structural analysis of platinum–palladium nanoparticles dispersed on titanium dioxide to evaluate cyclo-olefines reactivity, *J. Alloys Compd.*, 495 (2010) 453–457.
- [32] M.Y. Abdelaal, R.M. Mohamed, Novel Pd/TiO<sub>2</sub> nanocomposite prepared by modified sol–gel method for photocatalytic degradation of methylene blue dye under visible light irradiation, *J. Alloys Compd.*, 576 (2013) 201–207.
- [33] T. Ben Nasr, H. Maghraoui-Meherzi, H. Ben Abdallah, R. Bennaceur, First principles calculations of electronic and optical properties of Ag<sub>2</sub>S, *Solid State Sci.*, 26 (2013) 65–71.
- [34] H. Shen, X. Jiao, D. Oron, J. Li, H. Lin, Efficient electron injection in non-toxic silver sulfide (Ag<sub>2</sub>S) sensitized solar cells, *J. Power Sources*, 240 (2013) 8–13.
- [35] Y. Sun, B. Zhou, Synthesis and characterization of a novel biodegradable thermoplastic shape memory polymer, *Mater. Lett.*, 64 (2010) 347–349.
- [36] Y. Sun, B. Zhou, P. Gao, H. Mu, L. Chu, Single-crystalline Ag<sub>2</sub>S hollow nanoparticles and their ordered arrays, *J. Alloys Compd.*, 490 (2010) L48–L51.
- [37] S. Hull, D.A. Keen, D.S. Sivia, P.A. Madden, M. Wilson, The high-temperature superionic behaviour of Ag<sub>2</sub>S, *J. Phys.: Condens. Matter*, 14 (2002) 9–17.

- [38] T. Minami, Recent progress in superionic conducting glasses, *J. Non-Cryst. Solids*, 95 (1987) 107–118.
- [39] S.W. Hu, J. Zhu, L. Wu, X.X. Wang, P. Liu, Y.F. Zhang, Z.H. Li, Effect of fluorination on photocatalytic degradation of Rhodamine B over  $\text{In}(\text{OH})_y\text{S}_z$ : promotion or suppression?, *J. Phys. Chem. C*, 115 (2011) 460–467.
- [40] Z.H. Li, H. Dong, Y.F. Zhang, T.T. Dong, X.X. Wang, J.Q. Li, X.Z. Fu, Effect of  $\text{M}^{2+}$  ( $\text{M} = \text{Zn}$  and  $\text{Cu}$ ) dopants on the electronic structure and photocatalytic activity of  $\text{In}(\text{OH})_y\text{S}_z$  solid solution, *J. Phys. Chem. C*, 112 (2008) 16046–16051.
- [41] Z.H. Li, T.T. Dong, Y.F. Zhang, L. Wu, J.Q. Li, X.X. Wang, X. Z. Fu, Studies on  $\text{In}(\text{OH})_y\text{S}_z$  solid solutions: syntheses, characterizations, electronic structure, and visible-light-driven photocatalytic activities, *J. Phys. Chem. C*, 111 (2007) 4727–4733.
- [42] B. Delfort, M. Born, A. Chive, L. Barre, Colloidal calcium hydroxide in organic medium: synthesis and analysis, *J. Colloid Interface Sci.*, 189 (1997) 151–157.
- [43] H.G. Shin, H. Kim, Y.N. Kim, H.S. Lee, Preparation and characterization of high surface area calcium hydroxide sorbent for  $\text{SO}_2$  removal, *Curr. Appl. Phys.*, 9 (2009) S276–S279.
- [44] S. Zhang, A new nano-sized calcium hydroxide photocatalytic material for the photodegradation of organic dyes, *RSC Adv.*, 4 (2014) 15835–15840.

## Supplementary material

Table S1  
BET surface area and band gap of  $\text{Ca}(\text{OH})_2$  and  $\text{Ag}/\text{Ca}(\text{OH})_2$  nanospheres

| Sample                                     | $S_{\text{BET}}$ ( $\text{m}^2/\text{g}$ ) | Band gap energy (eV) |
|--|--|----------------------|
| $\text{Ca}(\text{OH})_2$                   | 50   | 3.40                 |
| 0.2 wt% $\text{Ag}/\text{Ca}(\text{OH})_2$ | 45   | 3.07                 |
| 0.4 wt% $\text{Ag}/\text{Ca}(\text{OH})_2$ | 42   | 2.99                 |
| 0.6 wt% $\text{Ag}/\text{Ca}(\text{OH})_2$ | 40   | 2.88                 |
| 0.8 wt% $\text{Ag}/\text{Ca}(\text{OH})_2$ | 39   | 2.85                 |